Rigorous 3D inversion of tensor electrical and magnetic induction well logging data in inhomogeneous media

Alexander Gribenko and Michael S Zhdanov, University of Utah*

SUMMARY

In this paper we develop a method of 3D inversion of tensor electric and magnetic field data in induction well-logging applications. Our method is based on the integral equation EM field formulation. An efficient Fréchet derivative computation is achieved by applying the modified Born approximation. The inversion method is tested on several synthetic models. The results of inversion show that both magnetic and electric tensor components can be used in 3D inversion about a single borehole.

INTRODUCTION

We describe a method of 3D inversion of the tensor (multicomponent) induction well-logging data, applicable to both electric and magnetic field tensors. There is growing interest in developing advanced techniques for 3D interpretation and imaging of induction well-logging data from a single borehole. It was demonstrated in several publications (Kriegshauser et al., 2001; Zhdanov et al., 2004; Wang et al., 2003; Abubakar et al., 2006) that, the tensor induction well-logging (TIWL) instrument can be used both for studying the anisotropy of the formations penetrated by the borehole and for imaging 3D structures in the borehole vicinity. Gribenko and Zhdanov, 2007a, presented a method of 3D nonparametric inversion of the TIWL magnetic field data, based on localized quasi-linear (LQL) approximation (Zhdanov et al. 2004) and on rigorous updates of the domain electric field (Cox and Zhdanov, 2008).

In this work we extend our interest to not only the magnetic field but also to the electric field components generated by the magnetic dipole transmitters. We introduce a new rigorous method of TIWL data inversion based on integral equation (IE) forward modeling (Hursán and Zhdanov, 2002). The Fréchet derivative calculation is based on the modified Born approximation, which has been proven to be an effective and accurate technique for EM data inversion (Gribenko and Zhdanov, 2007b). As a result, the IE-based method of TIWL inversion requires just one forward modeling at every iteration step, which dramatically speeds up the computations and results in a relatively fast and economical inversion method. To obtain a stable solution of a 3D inverse problem we apply regularization method (Tikhonov and Arsenin, 1977) with an option of focusing stabilizing functional (Portniaguine and Zhdanov, 1999). This stabilizer helps generate a sharp and focused image of anomalous conductivity distribution. We use regularized conjugate gradient method (Zhdanov, 2002) to minimize parametric functional.

A new algorithm for 3D TIWL data inversion is tested on several models of typical 3D structures located in the vicinity of the borehole. One of the synthetic models considered in this paper is similar to the oil-water contact model presented by Abubakar et al. (2006).

ELECTRIC AND MAGNETIC INDUCTION TENSORS

Figure 1 shows schematically a TIWL instrument, containing three orthogonal transmitter coils and three orthogonal receivers. Figure 1 also shows the relations between the axes x',y',z' of the instrument coordinate frame and the axes x,y, and z, of the medium coordinate frame. The angle α between z and z' is a relative deviation of the instrument with respect to the medium, and angle β is the so-called relative bearing angle. Tensor rotations can be applied to transform field components from one coordinate system to another (Zhdanov, et al., 2001) Three vectors of electric fields due to each of the three

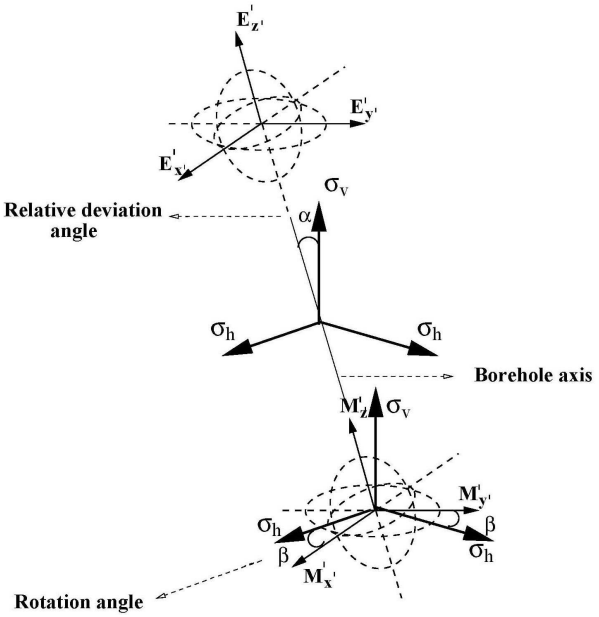

Figure 1: Three mutually orthogonal transmitter coils with moments $\mathbf{M}^{x'}$, $\mathbf{M}^{y'}$, and $\mathbf{M}^{z'}$, and three mutually orthogonal electrical receivers oriented parallel to the transmitters. The angle α between z and z' is a relative deviation of the instrument with respect to the medium, and β is the so-called relative bearing angle.

transmitters have three components each. These three vectors form an electric tensor given in the matrix representation as following:

$$\widehat{\mathbf{E}} = \begin{bmatrix} E_x^x & E_x^y & E_x^z \\ E_y^x & E_y^y & E_y^z \\ E_z^x & E_z^y & E_z^z \end{bmatrix}.$$

Similarly, three vectors of magnetic field due to each of the three transmitters form a magnetic induction tensor:

$$\widehat{\mathbf{H}} = \begin{bmatrix} H_x^x & H_x^y & H_x^z \\ H_y^x & H_y^y & H_y^z \\ H_z^x & H_z^y & H_z^z \end{bmatrix}.$$

The elements of these tensors are the EM field components for unit magnetic dipole transmitters in the directions of the basis vectors.

RIGOROUS 3D INVERSION OF TIWL DATA

The TIWL inverse problem

In the TIWL method, the EM field is excited by three mutually orthogonal magnetic transmitters. Three mutually orthogonal receivers record magnetic field at some distance from transmitter location. Another set of three mutually orthogonal receivers located at the same point can record electric fields generated by transmitters in the medium penetrated by the borehole (Peksen and Zhdanov, 2003). We can describe the forward TIWL problem by an operator equation:

$$\mathbf{d} = \mathbf{A}(\mathbf{m}), \tag{1}$$

where $\mathbf{d}$ stands for a *data vector* formed by the components of the electric and/or magnetic field recorded in the receivers, $\mathbf{A}$ is the nonlinear forward operator symbolizing the governing IE equations, and $\mathbf{m}$ is the vector of model parameters, which consists of the anomalous conductivities of the inversion cells $\Delta\sigma$. The purpose of the inversion is to recover the anomalous conductivity distribution $\Delta\sigma$ by solving the operator equation (1). The problem of finding $\Delta\sigma$ is ill posed, i.e., the solution can be nonunique and unstable. The conventional way of solving ill-posed inverse problems, according to regularization theory (Zhdanov, 2002), is based on minimization of the Tikhonov parametric functional:

$$P(\mathbf{m}) = \phi(\mathbf{m}) + \alpha S(\mathbf{m}) = min, \tag{2}$$

where $\phi(\mathbf{m}) = ||\mathbf{A}(\mathbf{m}) - \mathbf{d}||_2^2$ is the misfit functional between the predicted data $A(\mathbf{m})$ and the observed data $\mathbf{d}$, $s(\mathbf{m})$ is a stabilizing functional, and α is a regularization parameter.

Minimization of parametric functional

The common approach to minimization of the parametric functional $P(\mathbf{m})$ (2) is based on using gradient-type methods. In the case of a minimum-norm (MN) stabilizer, we can solve this minimization problem using the regularized conjugate-gradient (RCG) method. The algorithm of the RCG method can be summarized as follows (Zhdanov, 2002):

$$\mathbf{R}_n = \mathbf{A}(\mathbf{m}) - \mathbf{d}$$

$$\mathbf{l}_n^{\alpha n} = \mathbf{l}^{\alpha n}(\mathbf{m}_n) = \mathbf{Re}(\mathbf{F}_n^* \mathbf{W}_d^2 \mathbf{R}_n) + \alpha \mathbf{W}_m^2 (\mathbf{m} - \mathbf{m}_{apr})$$

$$\beta_n^{\alpha n} = \|\mathbf{l}_n^{\alpha n}\|^2 / \left\|\mathbf{l}_{n-1}^{\alpha n-1}\right\|^2$$

$$\tilde{\mathbf{I}}_n^{\alpha n} = \mathbf{l}_n^{\alpha n} + \beta_n^{\alpha n} \tilde{\mathbf{I}}_{n-1}^{\alpha n-1}$$

$$\tilde{\mathbf{I}}_0^{\alpha 0} = \mathbf{l}_0^{\alpha 0}$$

$$\tilde{k}_n^{\alpha n} = (\tilde{\mathbf{I}}_n^{\alpha n T} \mathbf{l}_n^{\alpha n}) / \left\{ \left\|\mathbf{W}_d \mathbf{F}_{mn} \tilde{\mathbf{I}}_n^{\alpha n}\right\|^2 + \alpha \left\|\mathbf{W}_m \tilde{\mathbf{I}}_n^{\alpha n}\right\|^2 \right\}$$

$$\mathbf{m}_{n+1} = \mathbf{m}_n - \tilde{k}_n^{\alpha n} \tilde{\mathbf{I}}_n^{\alpha n},$$

where $\tilde{k}_n^{\alpha n}$ is the step length, $\mathbf{l}_n^{\alpha n}$ is the gradient direction computed using an adjoint Fréchet derivative matrix, $\mathbf{F}_n^*$, and α_n are the subsequent values of the regularization parameter. Matrices $\mathbf{W}_d$ and $\mathbf{W}_m$ are the data and model parameter weighting matrices, respectively.

In the case of focusing inversion with minimum-support (MS) and minimum vertical-support (MVS) stabilizers (Zhdanov et al., 2007), we use the re-weighted regularized conjugate-gradient (RRCG) method introduced in Zhdanov (2002).

NUMERICAL EXAMPLES

Model 1

To test the developed algorithm we use the model shown in Figure 2. The model consists of one resistive and one conductive L-shaped anomaly located at different depths on opposite sides of the borehole. Figure 2 is a 3D image of the anomalous conductivity distribution, showing only anomalous bodies and positions of transmitters (stars) and receivers (circles). The background resistivity is of 20 Ohm-m, the resistivity of the conductive anomaly is 10 Ohm-m, and that of the resistive anomaly is 100 Ohm-m. We tested the algorithm with the

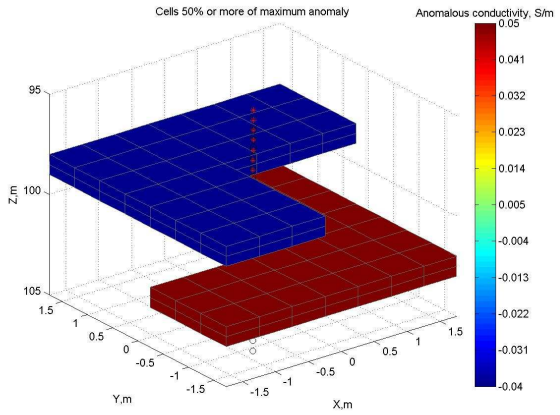

Figure 2: 3D view of true Model 1. The figure show the regions with the anomalous conductivity only. The stars show the transmitter locations, while circles represent the receivers.

data at multiple frequencies (1, 10, and 100 kHz), and multiple transmitter-receiver separations (0.33, 1, and 2 m). The synthetic observed TIWL data were computed by the IE code INTEM3D (Hursán and Zhdanov, 2002) for twenty one instrument positions with nine different components of the observed field at three frequencies and three separations, forming a total of 1701 data points. All nine components of the magnetic induction tensor and all nine components of the electric tensor were used in inversion as input data.

With appropriate data weighting, the developed algorithm allowed us to jointly invert magnetic and electric field components. We applied joint inversion to both magnetic and electric

induction tensors. Figure 3 shows a 3D image of the inversion result recovered by joint inversion. We have also achieved good data fit by joint inversion with the normalized error reaching less then 2% after 100 iterations.

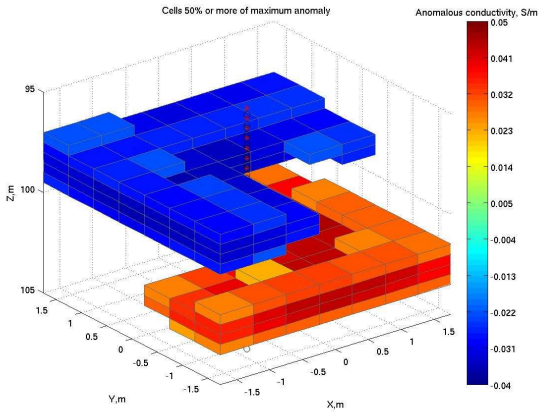

Figure 3: 3D image of the anomalous conductivity distribution recovered by the joint inversion of the magnetic and electric induction tensors for Model 1.

Model 2

The second model that we investigated is similar to the water-oil contact model considered by Abubakar and Habashy (2006). We use a homogeneous half-space with 20 Ohm-m resistivity as a background for this model. The formation consists of a water layer with 10 Ohm-m resistivity and a water-oil contact region. The conductivity of the oil is 100 Ohm-m and that of the water is 10 Ohm-m. Figure 4 represents a 3D view of the anomalous conductivity distribution in the true Model 2, and Figure 5 is a vertical section through the same model.

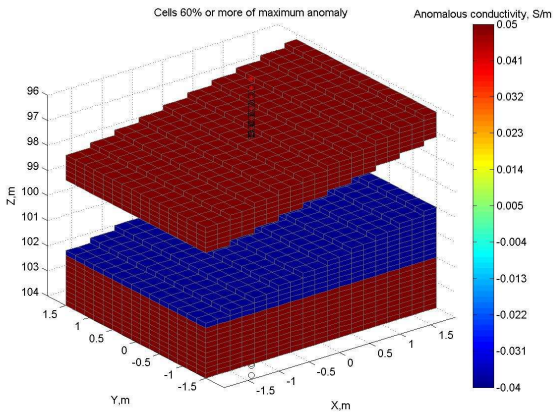

Figure 4: 3D view of the true Model 2. Only anomalous regions are shown. The stars show the transmitter locations, and the circles represent the receivers.

The joint inversion of magnetic and electric field tensors was applied to the model data. 20 Ohm-m half-space was used as initial model for the 3D inversion. Inversion domain consisted of 14440 cells 0.2x0.2x0.2 m^3 in size. Figure 6 shows the convergence curve. The normalized error reached less then 1% in 100 iterations. Figures 7 and 8 show the plots of the real and imaginary parts of the observed and predicted fields for one of the transmitter directions, Y, at 20 kHz frequency.

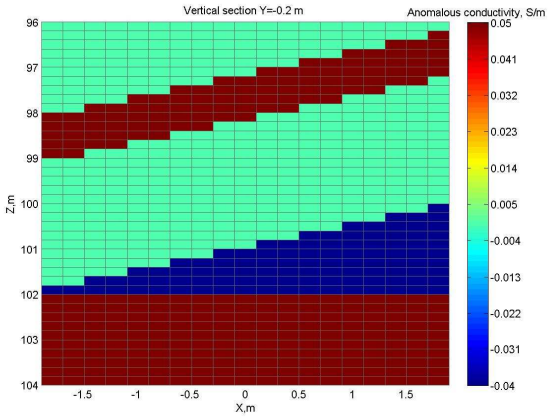

Figure 5: Vertical section through the true Model 2.

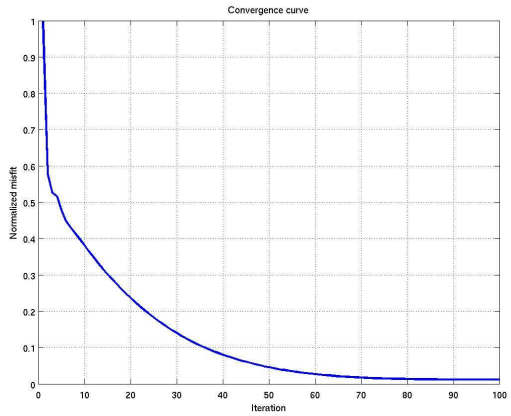

Figure 6: Normalized error behavior during joint inversion of the electric and magnetic field components for Model 2.

Figure 9 shows a 3D image of the inversion result, displaying only cells with anomalous conductivity larger then 50% of the maximum anomaly present in the distribution. Figure 10 represents vertical section through the inversion result. The inverted conductivity distribution is a good representation of the true model shown in Figures 4 and 5.

CONCLUSION

In this paper we have investigated a new method of induction logging based on both magnetic and electric field measurements. We have developed a new method of inversion of TIWL

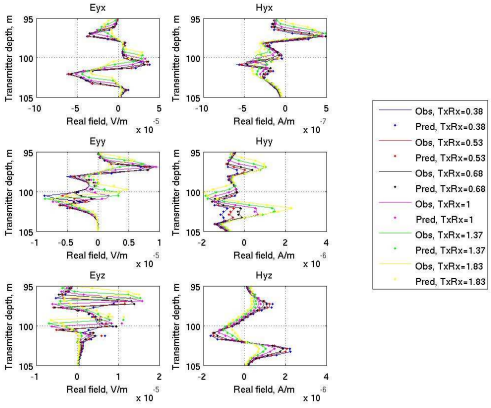

Figure 7: Plots of the real parts of the observed and predicted anomalous electric and magnetic fields excited by the Y-directed transmitter component for the Model 2 at a frequency of 20 kHz. The different colors correspond to different transmitter-receiver separations, the lines show the observed fields, and the dots represent the predicted fields.

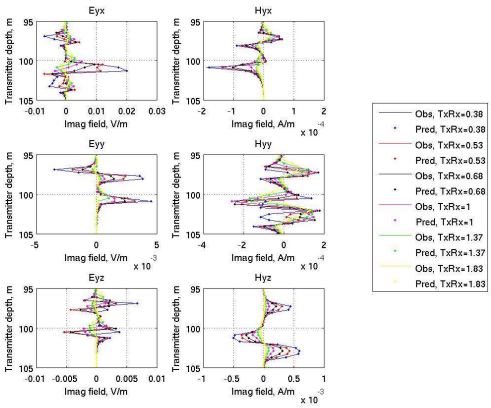

Figure 8: Plots of the imaginary parts of the observed and predicted anomalous electric and magnetic fields excited by the Y-directed transmitter component for the Model 2 at a frequency of 20 kHz. The different colors correspond to different transmitter-receiver separations, the lines show the observed fields, and the dots represent the predicted fields.

data based on IE forward modeling. The important component of this method is the Fréchet derivative calculation using the modified Born approximation. This technique allows us to simplify the inversion algorithm and to use just one forward modeling in every iteration step, which speeds up the computations and reduces the computer memory requirements. By introducing appropriate data weights we were able to jointly invert electric and magnetic components of the TIWL data successfully. The electric and magnetic components complement each other, providing a better image of the conductivity distribution in the formation penetrated by the borehole.

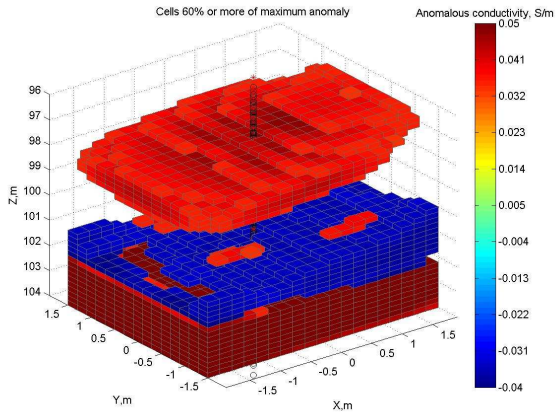

Figure 9: 3D image of the anomalous conductivity distribution recovered by the joint inversion of the magnetic and electric field components for Model 2.

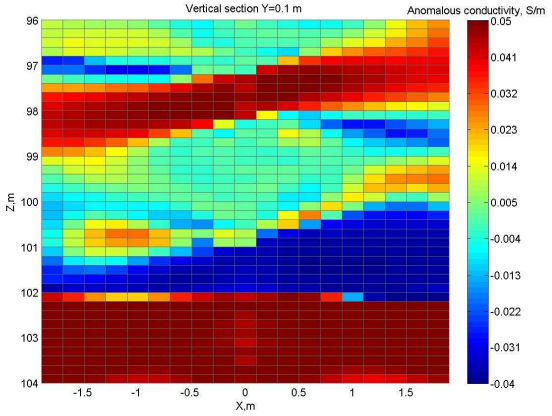

Figure 10: Vertical section through the anomalous conductivity distribution recovered by the joint inversion of the magnetic and electric field components for Model 2.

ACKNOWLEDGMENTS

The authors acknowledge the support of the University of Utah Consortium for Electromagnetic Modeling and Inversion (CEMI).

EDITED REFERENCES

Note: This reference list is a copy-edited version of the reference list submitted by the author. Reference lists for the 2009 SEG Technical Program Expanded Abstracts have been copy edited so that references provided with the online metadata for each paper will achieve a high degree of linking to cited sources that appear on the Web.

REFERENCES

Abubakar, A., T. M. Habashy, V. Druskin, L. Knizhnerman, and S. Davydycheva, 2006, A 3D parametric inversion algorithm for triaxial induction data: Geophysics, **71**, no. 1, G1–G9.

Cox, L. H., and M. S. Zhdanov, 2008, Advanced computational methods of rapid and rigorous 3-D inversion of airborne electromagnetic data: Communications in Computational Physics, **3**, 160–179.

Gribenko, A., and M. S. Zhdanov, 2007a, Regularized integral equation based inversion of tensor induction logging data in three-dimensional formations: 77th Annual International Meeting, SEG, Expanded Abstracts, 497–501.

———, 2007b, Rigorous 3D inversion of marine CSEM data based on the integral equation method: Geophysics, **72**, no. 2, 229–254.

Hursan, G., and M. S. Zhdanov, 2002, Contraction integral equation method in three-dimensional electromagnetic modeling: Radio Science, **37**, 1089–2002.

Kriegshauser, B., S. McWillams, O. Fanini, and L. Yu, 2001, An efficient and accurate pseudo 2-D inversion scheme for multicomponent induction log data: 71st Annual International Meeting, SEG, Expanded Abstracts, 376–380.

Peksen, E., and M. S. Zhdanov, 2003, The electric tensor in induction well logging: Proceedings of Annual Meeting of the Consortium for Electromagnetic Modeling and Inversion, 87–102.

Portniaguine, O. N., and M. S. Zhdanov, 1999, Focusing geophysical inversion images: Geophysics, **64**, 874–887.

Tikhonov, A. N., and V. Y. Arsenin, 1977, Solution of ill-posed problems: W. H. Winston and Sons.

Wang, T., Y. Liming, and O. Fanini, 2003, Multicomponent induction response in a borehole environment: Geophysics, **68**, 1510–1518.

Zhdanov, M. S., 2002, Geophysical inverse theory and regularization problems: Elsevier.

Zhdanov, M. S., A. Gribenko, and M. Čuma, 2007, Regularized focusing inversion of marine CSEM data using minimum vertical support stabilizer: 77th Annual International Meeting, SEG, Expanded Abstracts, 345–371.

Zhdanov, M. S., D. Kennedy, and E. Peksen, 2001, Foundations of tensor induction well-logging: Petrophysics, **42**, 588–610.

Zhdanov, M. S., E. Tartaras, and A. Gribenko, 2004, Fast 3-D imaging from a single borehole using tensor induction logging data: Petrophysics, **45**, 167–178.